Conformational Changes in Hemoglobin S (βE6V) Imposed by Mutation of the βGlu7–βLys132 Salt Bridge and Detected by UV Resonance Raman Spectroscopy

Laura Juszczak, Christophe Fablet, Veronique Baudin-Creuza, Sophie Lesecq-Le Gall, Rhoda Elison Hirsch, Ronald Nagel, Joel Friedman, Josée Pagnier

THE JOURNAL OF BIOLOGICAL CHEMISTRY
Vol. 278, No. 9, Issue of February 28, pp. 7257–7263, 2003
Printed in U.S.A.

Conformational Changes in Hemoglobin S (βE6V) Imposed by Mutation of the βGlu^{7}–βLys^{132} Salt Bridge and Detected by UV Resonance Raman Spectroscopy*

Received for publication, January 22, 2002, and in revised form, December 13, 2002
Published, JBC Papers in Press, December 16, 2002, DOI 10.1074/jbc.M200691200

Laura J. Juszczak‡§, Christophe Fablet§¶‖, Veronique Baudin-Creuza¶, Sophie Lesecq-Le Gall¶, Rhoda Elison Hirsch‡‡, Ronald L. Nagel‡**, Joel M. Friedman‡§§, and Josée Pagnier¶**

*From the ‡Department of Physiology and Biophysics, Albert Einstein College of Medicine, Bronx, New York 10461, the **Department of Medicine, Division of Hematology, Albert Einstein College of Medicine, Bronx, New York 10461, the ‡‡Department of Anatomy and Structural Biology, Albert Einstein College of Medicine, Bronx, New York 10461, and ¶INSERM, Unité 473, 84 rue du Général Leclerc, 94276 Le Kremlin-Bicêtre, France*

The impact upon molecular structure of an additional point mutation adjacent to the existing E6V mutation in sickle cell hemoglobin was probed spectroscopically. The UV resonance Raman results show that the conformational consequences of mutating the salt bridge pair, βGlu^{7}–βLys^{132}, are dependent on which residue of the pair is modified. The βK132A mutants exhibit the spectroscopic signatures of the R → T state transition in both the "hinge" and "switch" regions of the $\alpha_1\beta_2$ interface. Both singly and doubly mutated hemoglobin (Hb) βE7A exhibit the switch region signature for the R → T quaternary state transition but not the hinge signature. The absence of this hinge region-associated quaternary change is the likely origin of the observed increased oxygen binding affinity for the Hb βE7A mutants. The observed large decrease in the W3 α14β15 band intensity for doubly mutated Hb βE7A is attributed to an enhanced separation in the A helix-E helix tertiary contact of the β subunits. The results for the Hb A βGlu^{7}–βLys^{132} salt bridge mutants demonstrate that attaining the T state conformation at the hinge region of the $\alpha_1\beta_2$ dimer interface can be achieved through different intraglobin pathways; these pathways are subject to subtle mutagenic manipulation at sites well removed from the dimer interface.

Sickle cell hemoglobin (Hb S,[1] β6(A3) Glu → Val) exhibits the property of anomalous and pathologic self-assembly. DeoxyHb S forms polymers in the erythrocyte, which leads to microvascular blockage, organ damage, and often premature death. Structure-based drug design requires knowledge of optimal polymer disruption sites. The specific interaction in the Hb S polymer involves the steric fit of the mutated hydrophobic β6 donor site in a hydrophobic acceptor site located in an adjacent Hb S tetramer. It is well known that the hydrophobicity and the stereospecificity of the donor site are essential to the initiation of the polymerization.

Lesecq *et al.* (1, 2) have been investigating whether modification of the polarity close to the β6 site could influence the packing of the donor and acceptor sites, thus modifying the polymerization process. Replacing the hydrophilic Glu β7(A4) residue with a hydrophobic Ala residue resulted in a decreased polymerization of the doubly mutated rHb βE6V/E7A. It was postulated (1, 2) that the loss of the normal salt bridge between βGlu^{7}(A4) and βLys^{132}(H10) in the rHb βE7A mutants might lead to an alteration in both the position and the mobility of the A helix, illustrated in Fig. 1. These alterations of the A helix might result in a misfit between the donor and acceptor sites, which could explain the observed diminution in polymerization. It follows from this hypothesis that modifying the other partner of the salt bridge, βLys^{132}(H10), should have similar consequences on polymerization (2).

Visible resonance Raman spectroscopy is very useful in providing detailed information relating to the influence of tertiary and quaternary structure upon specific heme-related vibrational degrees of freedom (3–7). Additionally, UV resonance Raman spectroscopy (UVRR) provides information about vibrational modes of aromatic residues within the globin. UVRR studies of hemoglobin from several research groups have shown a consistent pattern of tertiary and quaternary structure shifts coupled to spectral changes in specific tyrosine and tryptophan bands (8–17). In particular and most significantly, spectral features have been clearly identified that reflect the key determinants of the quaternary state, specifically in the "hinge" (βTrp^{37}) and "switch" (αTyr^{42}) regions of the $\alpha_1\beta_2$ interface. Band intensities also respond to the packing of the A helix against the E helix and to the integrity of the salt bridge-derived scaffolding that maintains interhelical separations, a feature that is indicative of different tertiary structures within a given quaternary structure. Thus, the UVRR technique allows us to couple modifications of both local and global elements of structure with observed functional changes. For ex-

* This work was supported in part by National Institutes of Health Grants PO1 GM58890 and R01 HL58247, American Heart Association Heritage Affiliate Grant 9950989T, and Institut National de la Santé et de la Recherche Médicale and the Association Recherche et Transfusion Contract 21-2000. The costs of publication of this article were defrayed in part by the payment of page charges. This article must therefore be hereby marked "*advertisement*" in accordance with 18 U.S.C. Section 1734 solely to indicate this fact.

We dedicate this paper to the memory of Josée Pagnier, colleague and friend. Fortunately, she was able to see this work completed. She remains in our memory as a long standing collaborator. One of us (R. L. N.) was involved in her thesis work and remembers her with affection and gratitude in the pursuit (with Dominique Labie) of the origin of the sickle gene in Africa.

§ These authors contributed equally to this work.

‖ Supported by the Délégation Génerale pour l'Armement (Ministère de la Défense).

§§ To whom correspondence should be addressed: Dept. of Physiology and Biophysics, Albert Einstein College of Medicine, 1300 Morris Park Ave., Bronx, New York 10461. Tel.: 718-430-3591; Fax: 718-430-8819; E-mail: jfriedma@aecom.yu.edu.

[1] The abbreviations used are: Hb, hemoglobin; Hb S, sickle cell hemoglobin; Hb A, wild type human hemoglobin A; rHb, recombinant Hb; IHP, inositol hexaphosphate; UVRR, ultraviolet resonance Raman.

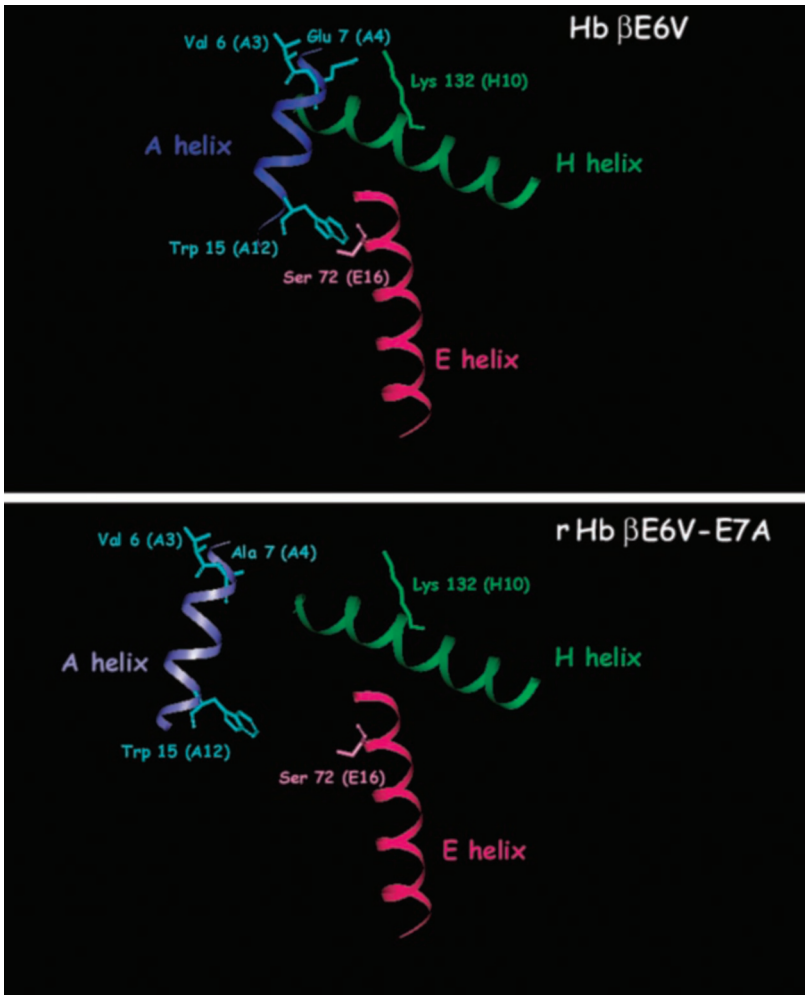

FIG. 1. **Schematic representation of the effects of the combination of βE6V and βE7A mutations on the conformation of the Hb helices A, E, and H.** The deoxygenated quaternary structure for Hb S was taken from the Protein Data Bank (structure number 2HBS). The βE7A mutation was introduced into the structure using the Hyperchem software program. *Top panel*, Hb βE6V. The E7-K132 salt bridge is intact, and the A helix W15-S72 hydrogen bond is present. *Bottom panel*, the additional E7A mutation breaks the salt bridge, resulting in a separation of the A and E helices.

ample, Hb C (β6(A3) Glu → Lys) is yet another naturally occurring mutant of Hb A, which forms crystals in erythrocytes. UVRR spectroscopy, in conjunction with other spectroscopic techniques, has been used to show that the effect of the β6 mutation is communicated to both the A helices and the central cavity where effectors such as inositol hexaphosphate (IHP) bind (18–20).

In this study, UVRR spectroscopy is utilized to probe the conformational consequences of disrupting the salt bridge between βGlu^{7}(A4) and βLys^{132}(H10) through examination of the tryptophan W3 and tyrosine Y8 bands, which are reporter bands for Hb tertiary and quaternary structure. The results for singly and doubly mutated recombinant Hbs βE6V, βE7A, βK132A, βE6V/E7A, and βE6V/K132A are compared with those for both wild type and recombinant Hb A (Hb A and rHb A, respectively). The deoxygenated and CO derivatives of each Hb species are examined, as is the CO derivative in the presence of IHP. The UVRR results reveal the impact of the βGlu^{7}–βLys^{132} salt bridge mutations on the positioning of the A helix and on the functioning of the quaternary β37 hinge, which suggest a molecular explanation for the macroscopic changes in polymerization and ligand binding for these mutants.

MATERIALS AND METHODS

Preparation of the Recombinant Hbs—The βE6V, βE7A, and βK132A mutations were introduced into the β-globin cDNA by site-directed mutagenesis using synthetic primers (Genset, France). The mutated β-globin subunits were produced as fusion proteins in *Escherichia coli*, using the expression vector pATPrcIIFXβ-globin (21). After extraction and purification, the fusion proteins were cleaved by digestion with bovine coagulation factor Xa (22). The presence of the mutation(s) was confirmed by reverse-phase high performance liquid chromatography of the tryptic digests and amino acid analysis of the abnormal peptides. The purified β-subunits were folded in the presence of cyanhemin and the partner α-subunits prepared from wild type Hb A, to form the tetrameric Hb $\alpha_2\beta_2$ (21, 23). The folded recombinant tetrameric Hbs were purified by preparative isoelectrofocusing on Ultrodex dextran gel using Ampholine (Amersham Biosciences, Uppsala, Sweden). Electrophoretic studies included electrophoresis on cellulose acetate and analytical isoelectrofocusing of the recombinant Hbs.

UVRR Spectroscopy—The Hb samples were all at a concentration of 0.5 mM heme in 50 mM Hepes at pH 7.35. 0.4 M sodium selenate was added as an internal standard, yielding a UVRR band at 834 cm^{-1}. Where applicable, the IHP was 0.75 mM or six times the Hb tetrameric concentration. The data were collected on samples chilled to 10 ± 4 °C to minimize photodamage. An argon laser system, described elsewhere (20), was used to generate the excitation wavelength of 228.9 nm with an incident laser power of 1.8 mW. Four 3-min acquisitions were accumulated for each ligation state of each Hb variant over a 820–1670 cm^{-1} frequency window. The UVRR data are averages of these four independent measurements. The measurements for the CO-ligated HbE6V/K132A with and without IHP were accumulated rather than averaged; the error bars are thus not shown in Fig. 4 for these species. The data frequency scale was calibrated with indene and toluene and is accurate to ±1 cm^{-1}. The issue of spectral reproducibility was addressed in the following manner: 1) The absorption spectra were collected before and after exposure to the UV laser beam. 2) If absorption changes were noted, the sequential UVRR acquisitions were examined for evidence of band changes. 3) Acquisitions that showed substantial changes were rejected and not included in the final UVRR average spectra. That is, separate acquisitions that were consistent in peak intensity and frequency as well as band shape were included in the averaged spectra. Spectral data were truncated to a 1530–1650 cm^{-1} frequency window, and the intensity was normalized at the W3 band (~1558 cm^{-1}) for each set of spectra in Figs. 2 and 3. The software

program Grams/32 AI, version 6.00 (Galactic Industries Corp., Salem, NH) was used to determine the Y8a and W3(α14β15) peak heights used in Table I (full width at half-maximum) using the subroutine, Peakstat, and for curve fits to the W3 band, from which band heights for the β37 shoulder at ~1548 cm^{-1} were determined. All W3 bands were fit to two curves of 0.7 Lorentzian/0.3 Gaussian band shape as the vibrational signature for the α14 and β15 Trps is coincidental and cannot be resolved; the second curve is for the β37 Trp. All of the band intensities given in Table I and Fig. 4 were normalized against the selenate 834 cm^{-1} peak. The numerical errors listed in Table I and the *error bars* shown in Fig. 4 were determined from the normalized peak intensities of the independent component acquisitions used for each averaged UVRR spectrum as measured by the aforementioned Peakstat subroutine. Common spectral processing techniques include smoothing to improve the signal-to-noise ratio (24); spectral smoothing, however, was not employed here.

RESULTS AND DISCUSSION

Hb A

The changes in Hb globin structure that accompany ligation at the heme can be followed by UVRR spectroscopy because of the critical sites occupied by several of the UV-resonating Trp and Tyr residues. Two of these are highly responsive to quaternary structural changes: βTrp^{37} and αTyr^{42} are located in the hinge and switch regions of the $\alpha_1\beta_2$ dimer interface, respectively. In addition, there is a tryptophan on the A helix of both the α (α14) and β (β15) subunits that provides a UVRR signature for the status of the packing distance between the A and E helices (25). For human wild type Hb A, the change in ferrous heme ligation state from fully ligated to fully deligated (deoxy) is accompanied by the R → T state quaternary structure transition. The conformational changes of the aromatic residues in the interface following the R → T state transition yield two major UVRR spectral changes. These are a ~2-cm^{-1} increase in frequency of the Y8a band from ~1615 to ~1617 cm^{-1} and an intensity increase of ~37% in the W3 shoulder (W3 β37) at 1549 cm^{-1} (7, 9). Several investigators have used these UVRR spectral changes to characterize the effect of site mutation on hemoglobin (6, 7, 9, 10, 12–15, 17, 20, 25–28). Thus, the association of these small spectral changes with specific changes in hemoglobin structure and ligation state is both well documented and consistent. The UVRR spectra shown in Figs. 2 and 3 have been truncated to highlight the 1530–1650 cm^{-1} frequency window. This spectral window contains the conformation-sensitive W3 and Y8a reporter bands.

The W3 band at ~1558 cm^{-1} has two contributions (9, 13, 27, 29). The central feature that peaks at ~1558 cm^{-1} is derived from the two A helix tryptophans (α14 and β15), whereas the R → T state sensitive shoulder at ~1550 cm^{-1} originates from βTrp^{37}. Intensity changes in the central peak of the W3 band at ~1558 cm^{-1} have been shown to originate from variations in the hydrogen bond between the A helix tryptophans and their hydrogen-bonding partners on the E helix (25). Increased and decreased intensities correlate with increases and decreases in hydrogen bond strength, respectively. Modulation of the hydrogen bond strength is attributed to changes in the distance between the two helices.

The intensity for the ~1550 cm^{-1} shoulder on the W3 band increases as the hinge region of the $\alpha_1\beta_2$ interface undergoes an R → T state transition, reflecting the changes in the hydrogen bonding pattern of βTrp^{37} with αAsp^{94}. Thus, the W3 band provides information on both the functionally important hinge region of the $\alpha_1\beta_2$ interface and the packing of the A and E helices. The tyrosine-derived Y8a band at ~1616 cm^{-1} shows a ~1–2-cm^{-1} shift to higher frequency when liganded R-state Hb A is converted to the deoxy T state (9, 29). This frequency shift originates primarily from αTyr^{42} (13, 17, 28) in the switch region of the $\alpha_1\beta_2$ interface. The intensity of this band has been correlated with the integrity of the scaffolding supporting the H helices.

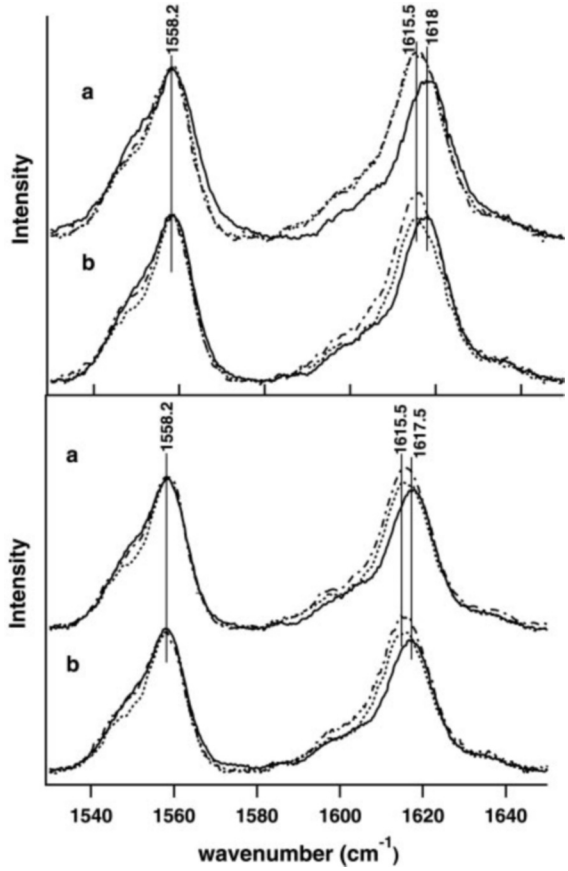

FIG. 2. **W3 (~1558 cm^{-1}) and Y8 (~1615 cm^{-1}) UVRR bands for hemoglobin A (*top panel*, *set a*, wild type; *set b*, recombinant) and hemoglobin S (*bottom panel*, *set a*, wild type; *set b*, recombinant).** *Solid line*, deoxygenated Hb; *broken line*, CO ligated Hb; *dotted* and *dashed line*, CO ligated Hb in the presence of IHP. The spectra have been normalized to the W3 peak.

The intensity of the UVRR spectra in each set in Figs. 2 and 3 have been normalized at the W3 peak to clarify the differences in the β37 shoulder at 1548 cm^{-1}. Both wild type Hb A and rHb A (Fig. 2, *top panel*, *sets a* and *b*, respectively) yield the well documented Y8a frequency increase (2.9 and 1.8 cm^{-1}, respectively; Table I), and the W3 β37 band intensity increase (0.43 and 0.44, respectively; Table I) associated with the R → T state transition, as discussed above. The spectral *difference* between the W3 β37 bands for the two hemoglobin ligation states is 1 order of magnitude above the noise level of the constituent spectral acquisitions. For both species of Hb A, ligation results in an increase of intensity for the W3 α14β15 band (Fig. 4*a* and Table I), whereas the Y8a band intensity increases for ligated wild type Hb A only (Fig. 4*b* and Table I). Addition of a 5-fold excess of the effector, IHP, to ligated forms of both Hb As results in an enhancement of the W3 β37 band intensity, which is indicative of a more T state-like hinge region, but apparently has little or no effect on the Y8a band position, which remains R state like (Fig. 2, *top panel*, *sets a* and *b*, and Table I). The addition of IHP has a large enhancement effect on the Y8a band intensities of both ligated Hb As (Fig. 4*b* and Table I) and on the W3 α14β15 band intensity of wild type Hb A (Fig. 4*a* and Table I).

Hb S (βE6V)

The upshift in the Y8 band frequency and the W3 β37 band intensity increase accompanying the R → T state transition for both Hb As are also found in the UVRR results for wild type Hb S and rHb S (Fig. 2, *bottom panel*, *sets a* and *b*, respectively,

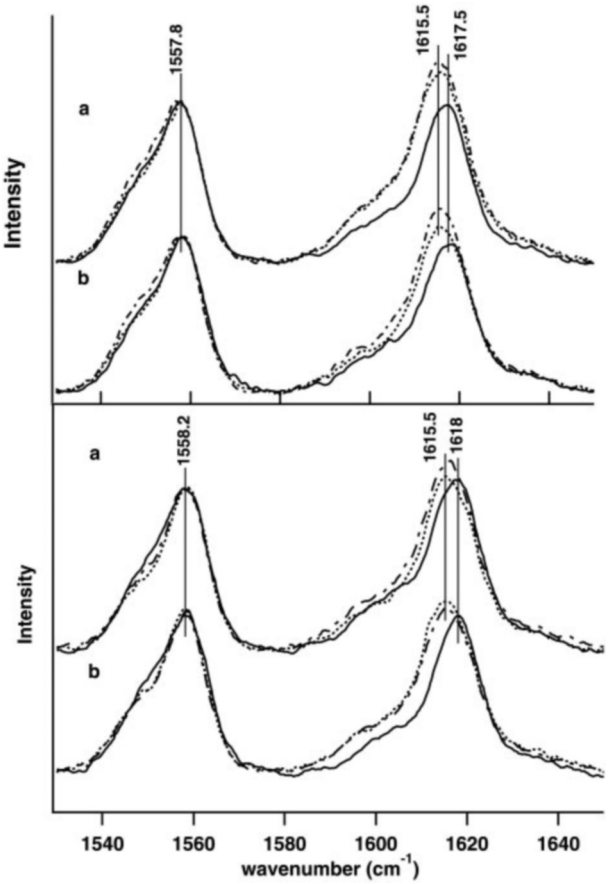

FIG. 3. **W3 (~1558 cm^{-1}) and Y8 (~1615 cm^{-1}) UVRR bands for hemoglobin mutants.** *Top panel*, *set a*, rHb E7A; *set b*, rHb E6V/E7A. *Bottom panel*, *set a*, rHb K132A; *set b*, rHb E6V/K132A. *Solid line*, deoxygenated Hb; *broken line*, CO ligated Hb; *dotted* and *dashed line*, CO ligated Hb in the presence of IHP. The spectra have been normalized to the W3 peak.

and Table I). The W3 β37 band intensity increase for deoxy wild type Hb S is comparable (0.45) with that obtained for either species of deoxy Hb A (0.43–0.44), whereas the intensity increase obtained for deoxy rHb S is higher (0.53) (Table I). Conversely, ligation, which corresponds to the T $\rightarrow$ R state transition, results in intensity increases for both the W3 and Y8 bands of wild type Hb S (0.19 and 0.26, respectively; Table I) and for those of rHb S (0.13 for W3 and 0.17 for Y8a; Fig. 4 and Table I). Addition of IHP to wild type COHb S yields little, if any, decrease in the W3 band intensity (Fig. 4*a* and Table I) and an unchanged Y8 band intensity (Fig. 4*b* and Table I). For COrHb S, the addition of IHP results in an increase in the Y8a band (Fig. 4*b* and Table I).

rHb βE7A

The characteristic Y8a frequency upshift accompanying the R $\rightarrow$ T state transition is also manifest by rHb βE7A (Fig. 3, *top panel*, *set a*, and Table I). The usual W3 β37 intensity increase, however, is not found in the UVRR results for this rHb mutant (Fig. 3, *top panel*, *set a*, and Table I). The W3 α14β15 and Y8a band intensities for deoxy rHb βE7A are similar in magnitude to those of wild type deoxyHb A (Fig. 2, *top panel*, *set a*), whereas ligation to rHb βE7A yields a small decrease in the W3 α14β15 band intensity and no change in the Y8a band intensity (Fig. 4 and Table I). The addition of IHP to COrHb βE7A leads to intensity increases in the Y8a and W3 β37 bands: a 0.36 increase in Y8a relative to the Y8a band of deoxy rHbβE7A (Table I) and a 0.16 increase in the W3 β37 band, comparable with the 0.11 band increase found in the results for wild type COHb A + IHP (Table I). Under the same conditions, the W3 α14β15 band intensity has merely been restored to its deoxy value (Fig. 4*a* and Table I).

rHb βE6V/E7A

The UVRR results for rHb βE6V/E7A following the R $\rightarrow$ T state transition are similar to those for rHb βE7A; the Y8a frequency upshift occurs, but the W3 β37 band intensity increase does not (Fig. 3, *top panel*, *set b*, and Table I). This double mutation results in the lowest deoxy W3 α14β15 and Y8a band intensities observed for this set of Hbs (Fig. 4). Ligation substantially increases the intensities of both bands (Fig. 4 and Table I). Addition of IHP to the ligated species has a small effect on the intensity of the W3 α14β15 band (Fig. 4*a*) but results in a substantially enhanced W3 β37 band intensity (Fig. 3, *top panel*, *set b*, and Table I). The intensity of the Y8a band is minimally influenced by the addition of IHP to CO rHb βE6V/E7A (Fig. 4*b* and Table I).

rHb βK132A

The K132A mutation did not affect the Y8 band shift associated with the R $\rightarrow$ T state transition (Fig. 3, *bottom panel*, *set a*, and Table I). The W3 β37 band intensity increase associated with this transition, however, was greater than that seen for wild type HbA (Fig. 3, *bottom panel*, *set a*, and Table I). Both the W3 α14β15 and Y8a band intensities for deoxy rHb K132A are higher than those for wild type deoxyHb A (Fig. 4). Ligation to rHb K132A further enhances both of these bands, and the addition of IHP leads to additional band intensity increases, with a nearly 2-fold Y8a band increase for CO rHb K132A + IHP over that of wild type deoxyHbA (Fig. 4 and Table I). In contrast to the results for the ligated rHb mutants discussed above, the addition of IHP to CO rHb K132A does not result in an increase in the W3 β37 band (Fig. 3, *bottom panel*, *set b*, and Table I).

rHb βE6V/K132A

The UVRR results for the R $\rightarrow$ T state transition of rHb βE6V/K132A are similar to those for rHb K132A (Fig. 3, *bottom panel*, and Table I). Generally, the W3 α14β15 and Y8a band intensities for deoxy rHb βE6V/K132A are greater than those observed for wild type deoxyHbA (Fig. 4). Ligation, however, has little effect on either the W3 α14β15 band intensity or on the intensity of the Y8a band (Fig. 4). The addition of IHP enhances both the W3 α14β15 and Y8a bands, but the Y8a band for ligated rHb βE6V/K132A is reduced relative to that for ligated rHb K132A (Fig. 4*b*). As for CO rHb K132A, the addition of IHP does not enhance the intensity of the W3 β37 band (Fig. 3, *bottom panel*, *set b*, and Table I).

Two categories of UVRR spectral differences are observed in comparing the different Hb derivatives. One set is associated with R $\rightarrow$ T state differences and is comprised of a Y8a band shift and a W3 β37 intensity increase. The former change is observed when comparing the deoxy and CO derivatives for all the Hb species examined in the present study, whereas the latter is observed for all species *except* the E7A mutants. The second set of spectroscopic changes consists of intensity changes in the W3 α14β15 and Y8a UVRR bands when comparing both the different derivatives (ligation state) of a given Hb and the same derivative from different Hbs.

None of the Hb S-related mutations discussed here eliminate the Y8 band 1.5–3 cm^{-1} upshift (Figs. 2 and 3 and Table I) associated with the switch motion of the αTyr^{42}(C7) during the R $\rightarrow$ T state transition. This upshift has been shown to originate largely from βAsp^{99}(G9) hydrogen bond donation to αTyr^{42}(C7) upon Hb ligation (9, 13, 30). Similarly, the W3 β37

TABLE I
UVRR Y8a Band Peak Position Shift ($\Delta\vartheta_{Y8a}$) and Band Height Changes ($\Delta I/I_0$)

		$\Delta\vartheta_{Y8a}$[a]	$\Delta I_{Y8a}/I_0$[b]	$\Delta I_{W3\alpha14/\beta15}/I_0$[c]	$\Delta I_{W3\beta37}/I_0$[d]
Wild type Hb A	deoxy	2.9			0.43 (0.38/0.5)
	CO		0.38 (0.37/0.39)	0.19 (0.18/0.20)	
	CO + IHP	−0.2	0.68 (0.64/0.77)	0.45 (0.44/0.46)	0.11 (0.11/0.12)
rHb A	deoxy	1.8			0.44 (0.42/0.45)
	CO	0	0.01 (0.01/0.01)	0.13 (0.13/0.14)	
	CO + IHP	0.4	0.36 (0.34/0.37)	0.17 (0.16/0.18)	0.22 (0.21/0.23)
Wild type Hb S	deoxy	1.8			0.45 (0.45/0.46)
	CO	0.4	0.26 (0.24/0.28)	0.19 (0.17/0.22)	
	CO + IHP	0.3	0.27 (0.26/0.29)	0.11 (0.11/0.11)	0.38 (0.37/0.41)
rHb S	deoxy	1.6			0.53 (0.50/0.57)
	CO	0.2	0.17 (0.15/0.18)	0.13 (0.12/0.14)	
	CO + IHP	−0.2	0.35 (0.34/0.36)	0.17 (0.16/0.18)	0.22 (0.20/0.24)
rHb E7A	deoxy	2.1			0.02 (0.02/0.02)
	CO	0.7	0.04 (0.04/0.04)	−0.15 (−0.16/−0.14)	
	CO + IHP	0	0.36 (0.35/0.37)	0.07 (0.06/0.07)	0.16 (0.15/0.19)
rHb E6V/E7A	deoxy	1.4			0.09 (0.08/0.10)
	CO	0.1	0.41 (0.39/0.44)	0.26 (0.23/0.32)	
	CO + IHP	−0.1	0.57 (0.54/0.60)	0.27 (0.24/0.29)	0.36 (0.35/0.37)
rHb K132A	deoxy	1.8			0.50 (0.49/0.52)
	CO	0.3	0.25 (0.24/0.26)	0.26 (0.25/0.27)	
	CO + IHP	0.2	0.47 (0.42/0.54)	0.34 (0.29/0.38)	0.05 (0.05/0.05)
rHb E6V/K132A	deoxy	2.2			0.49 (0.45/0.51)
	CO	0.2	0.08	−0.02	
	CO + IHP	0.1	0.33	0.21	0.06

[a] $\Delta\vartheta_{Y8a} = \vartheta_x - \vartheta_{COHbA}$, $\vartheta_{COHbA} = 1615.2\ cm^{-1}$, and x is the species of Hb.
[b] $\Delta I_{Y8a}/I_0 = (I_{Y8a(COHb \pm IHP)} - I_0/I_0$, where $I_0 = I_{Y8a(deoxyHb)}$ for each species of Hb; all intensities have been normalized to the internal selenate standard.
[c] $\Delta I_{W3\alpha14/\beta15}/I_0 = (I_{W3\alpha14/\beta15(COHb \pm IHP)} - I_0)/I_0$, where $I_0 = I_{W3\alpha14/\beta15(deoxyHb)}$ for each species of Hb; all intensities have been normalized to the internal selenate standard.
[d] $\Delta I_{W3\beta37}/I_0 = \{[I_{W3\beta37}(Hbx)/I_{W3\alpha14\text{-}\beta15}(Hbx)] - [I_{W3\beta37}(COHbx)/I_{W3\alpha14\text{-}\beta15}(COHbx)]\}/[I_{W3\beta37}(COHbx)/I_{W3\alpha14\text{-}\beta15}(COHbx)]$, where x = species of Hb.
All intensity errors are given in parentheses.

band intensity increase, associated with the R → T state transition hinge motion at the $\alpha_1\beta_2$ interface (9), is seen in all the deoxy *versus* CO UVRR comparisons for the Hbs discussed here *except* for those with the E7A mutation (Figs. 2 and 3 and Table I). The W3 β37 band intensity increase has been associated with changes in the hydrogen bond between βTrp^{37}(C3) and αAsp^{94}(G1).

The addition of IHP to the CO derivatives results in small to moderate intensity increases for the W3 β37 shoulder for the Hb A, the Hb S species, and the E7A mutants but not for the K132A mutants (Figs. 2 and 3 and Table I). This intensity increase is in the direction of the R → T state transition-associated change. Several features are worthy of additional comment. It is indeed intriguing that for the E7A mutants, deoxygenation does not induce the typical R → T state transition-associated intensity increase in the W3 β37 band, but addition of IHP to the liganded derivative does. This observation indicates that there are clearly multiple intraglobin pathways for inducing changes at the hinge region of the dimer interface. The concept of multiple pathways is further substantiated by the results from the E132A mutants, which exhibit the reverse effect in that deligation but not the addition of IHP induces the R → T state transition-associated changes in the hinge sensitive W3 β37 shoulder. The results also show that changes in the hinge and switch regions are necessarily coupled because under the present conditions the addition of IHP does not result in the Y8a, R → T state-associated frequency shift. At the significantly lower pH of 6.3, IHP addition to the CO derivatives of HbA, rHb βE6V, and rHb βE7A also induces the Y8 band to partially upshift toward the T state value (data not shown).

R → T state Transition-associated Spectral Changes

Effect of the βE7A Mutation—The rHb βE7A mutation replaces a negatively charged residue with one that is noncharged and aliphatic, resulting in the loss of the salt bridge with the positively charged residue, βLys^{132}. Based on the W3 β37 UVRR results presented here, it appears that the disruptive effect of the uncompensated βLys^{132} charge on the hinge region of the $\alpha_1\beta_2$ interface is equivalent to the loss of the R → T state transition (Fig. 3, *top panel*). One possible communication pathway for this disruption to the βTrp^{37} hinge region is through βGln^{131}, which is adjacent to the β7 salt bridge partner, βLys^{132}, and is noncovalently linked to the interfacial αHis^{103} (31). This disruption of the quaternary contacts within the hinge region of the T state $\alpha_1\beta_2$ interface is consistent with the increase in oxygen affinity of the rHb E7A mutants reported by Lesecq *et al.* (1). Disruption of the hinge via mutagenic manipulation of β37 has been shown to enhance the ligand binding properties of the T state and reduce proximal strain at the heme (32, 33).

Effect of the βK132A Mutation—The effect of eliminating the β7–β132 salt bridge by replacing positively charged Lys^{132} with uncharged, aliphatic Ala is to enhance the R → T transition state-associated W3 β37 band intensity increase *vis à vis* that for wild type Hb A (Table I). Thus, the loss of charge at β132 creates a "hyper" T state hinge signature. This result, in association with those from the βE7A mutant, indicates that uncompensated charge at the β132 site destabilizes the T state hinge, whereas loss of charge at this site enhances the T state hinge, and the function of the salt bridge is to modulate the T state hinge by offsetting the charge at β132.

Y8a and W3 α14β15 Band Intensity Changes—The relative intensities of the W3 and Y8 bands appear to follow a pattern upon comparing derivatives of a given Hb. Although there are several exceptions (Fig. 4), the intensity of the W3 and Y8 bands generally increases in the sequence of deoxy:CO:CO + IHP.

Doubly Mutated rHb βE6V/E7A—As shown in Fig. 4 and Table I, the UVRR spectra obtained from deoxy rHb βE6V/E7A show the most pronounced intensity decrease for both the W3 α14β15 and Y8 bands. Building on the findings of Spiro and co-workers (9, 12, 13, 25), this intensity decrease in the W3 α14β15 peak can be explained by a separation of the A helix

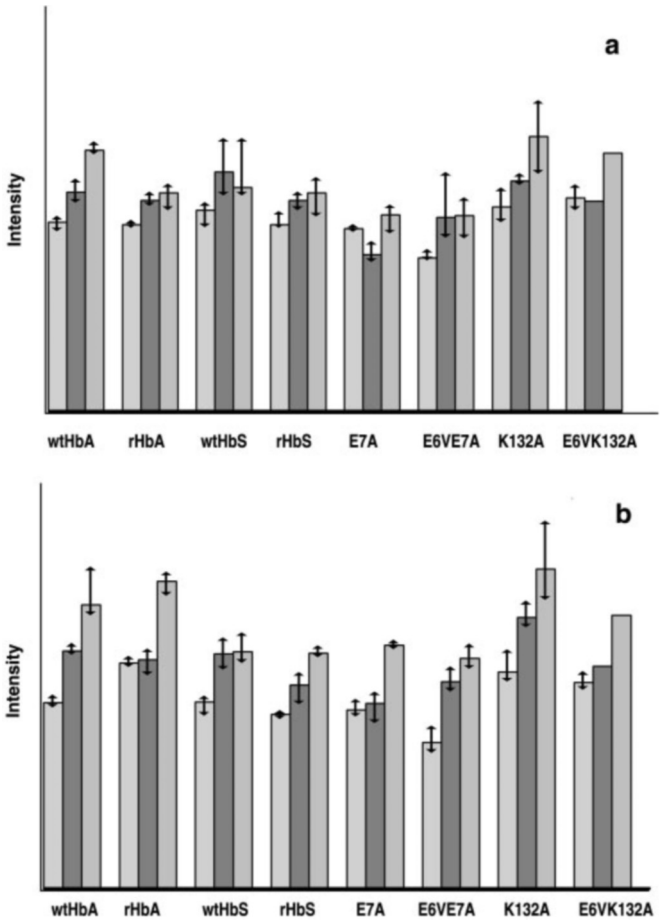

FIG. 4. **Normalized (834 cm^{-1}) band intensities from 229 nm excited UVRR spectra of Hb wild type and mutant species, pH 7.35, are shown.** In each group of columns, the *first column* shows the deoxy ligation state, the *second column* is CO-ligated, and the *third column* is CO-ligated in the presence of the effector IHP. *a*, W3 $\alpha 14\beta 15$ band. *b*, Y8a band.

from the E helix of the β chains caused by the combined change in the polarity and hydrophobicity of both the $\beta 6$ and $\beta 7$ residues, as illustrated in Fig. 1. It is not clear whether changes in hydration induce slight changes in the α helix itself. The $\alpha 14$ and $\beta 15$ tryptophan residues are not distinguishable by UVRR spectroscopy, but given that the mutations studied here are located on the β chain, all of the differences observed on the W3 $\alpha 14\beta 15$ main band can be reasonably assigned to βTrp^{15} (14). βTrp^{15} is an A helix residue situated in the crevice formed by the A and E helix. It normally forms a hydrogen bond with βSer^{72} of the E helix in both the deoxy and oxy structure (Fig. 1, *top panel*). A decrease in the intensity of the 1558-cm^{-1} band reveals a weakening of this hydrogen bond. In a study of C terminally deleted Hb A, Wang and Spiro (7) observed intensity increases in the W3 $\alpha 14\beta 15$ (A12) peak of both deoxy and ligated Hb A, which they attribute to a collapse of the A helix toward the E helix. This collapse is purported to originate from the loss of the C-terminal anchor of the H helix. The plausible claim was made that the H helix acts as a scaffold for the A helix, which keeps the A helix separated from the E helix (Fig. 1). A weakening of the scaffolding through changes in the hydrogen bonds and salt bridges of the H helix allows the A helix to pack more tightly against the E helix, thus allowing for a stronger βTrp^{15}(A12) to βSer^{72}(E16) hydrogen bond. Hirsch *et al.* (19) observed a decreased intensity of the W3 $\alpha 14\beta 15$ band of Hb C, where $\beta 6$ glutamic acid is replaced by a lysine residue. These authors demonstrated a weakening of the βTrp^{15}(A12)–βSer^{72}(E16) hydrogen bond, which is suggestive of a displacement of the A helix away from the E helix.

In the present study, the deoxy rHb βE6V/E7A Y8a band is 16% less intense than that observed for deoxy rHb S (Fig. 4*b* and Table I). Y8a band intensity changes can reasonably be attributed to either or both of the two penultimate tyrosine residues in the Hb molecule, αTyr^{140} and βTyr^{145}. Both residues are integral parts of the scaffolding linking the H and A helices. The Y8a intensity changes observed in the present study are likely to originate from βTyr^{145}. βTyr^{145}(HC2) occupies the pocket made by the H and F helices in deoxy HbA and deoxy Hb S and forms a hydrogen bond with βVal^{98}(FG5), which contributes to the scaffolding of the A helix by the H helix. The decrease in the deoxy rHb βE6V/E7A Y8a band intensity (Fig. 4*b*) is postulated to arise from a weakening of the βTyr^{145}–βVal^{98} hydrogen bond through a shift in the H helix.

Single Mutants, rHb βE7A and βK132A and Doubly Mutated rHb βE6V/K132A: Involvement and Role of the Salt Bridge $\beta 7$–$\beta 132$—The W3 and Y8a bands intensities for deoxy rHb βE7A are similar to those of deoxy rHb S (Fig 4 and Table I). No weakening of the hydrogen bond involving βTrp^{15}(A12) and βSer^{72}(E16) can be inferred. This result suggests that the absence of the salt bridge between βGlu^{7}(A4) and βLys^{132}(H10) *per se* does not influence the separation of the A and E helices and the A and H helices.

This claim is supported by the results from mutants rHb βK132A and rHb βE6V/K132A. The W3 and Y8a bands for the deoxy derivative of these rHbs exhibit increased intensities compared with that for deoxy rHb S (Fig. 4 and Table I). In these mutants, the $\beta 7$ (A4)–$\beta 132$ (H10) salt bridge is also absent, whereas the βTrp^{15}(A12)–βSer^{72}(E16) hydrogen bond is apparently strengthened, showing a tighter packing of the A helix against the E helix as follows from the discussion above. The other ligation state derivatives of these mutants show either no additional change or a further increase in the W3 and Y8a bands intensities (Fig. 4 and Table I). It appears that complete loss of the charge at position $\beta 132$ results in a loss of the A-H scaffolding with a concomitant decrease in the spacing between the A and E helices. It follows that the $\beta 7$–$\beta 132$ salt bridge modulates the charge at the $\beta 132$ residue in a way that allows for the appropriate degree of interhelical scaffolding and proper behavior of the hinge region at the dimer interface.

Importance of the Hydrogen Bond Involving βTyr^{145} and βVal^{98}—In a study of βTyr^{145} mutants, Ishimori *et al.* (34) showed that the presence of the phenolic side chain in the H-F pocket is a contributing factor to T state stability, whereas the hydrogen bond strength between βTyr^{145}(HC2) and βVal^{98}(FG5) is a modulating factor for the extent of proximal strain within the T state. Loss of the hydrogen bond is associated with a decrease in proximal strain as reflected in an increase in the frequency of the iron-proximal histidine-stretching mode for the deoxy derivative of the βY145F mutant. A subsequent study by Togi and co-workers (35) showed that this hydrogen bond is also important in stabilizing the R → T transition state. Loss of the hydrogen bond increased the energy of the transition state and thereby slowed the R → T state transition.

The current study suggests that the A helix mutations E6V and E7A lead to modifications of the scaffolding through changes in hydrogen bonds and salt bridges to the H helix. The decrease in Y8a UVRR band intensity observed for the deoxy rHb βE7A mutants may indicate a weakening of the βTyr^{145}(HC2)–βAsp^{98}(FG5) hydrogen bond because of the aforementioned modifications. Based on the $\beta 145$ mutant studies described above, this proposed bond weakening should re-

sult in a higher oxygen affinity for Hb, which has been observed for singly and doubly mutated Hb βE7As (1).

Conclusion

The spectroscopic results in this study show that the consequences of disrupting the salt bridge between βGlu^{6} and βLys^{132} is a function of which contributing residue is altered. The salt bridge clearly does not function simply as a taut spring linking two helices together, which when disrupted results in an automatic separation of the spring-linked elements. The salt bridge appears to modulate the effect of the charge of βLys^{132}. Complete loss of the charge, as occurs in the βK132A mutants, results in spectroscopic signatures for a collapse of the scaffolding supporting the A and H helices leading to a more "compressed" overall structure. The resulting structure is still capable of undergoing the full range of R → T state transition-associated hinge and switch motions as reflected in the UVRR spectrum. There are also spectroscopic indications that the charge at β132 effects the stability of the T state hinge region of the $\alpha_1\beta_2$ dimer interface. Both the single and double βE7A mutants, where the charge on β132 is fully unshielded, fail to show the hinge region-associated W3 β37 band intensity increase for the R → T state transition that is seen for all the other mutants, including βK132A. The absence of the R → T state change in the hinge region is a likely factor in the increased oxygen binding affinity observed for the rHb βE7A mutants. Thus, too little shielding of the charge at βLys^{132} results in an altered T state hinge region of the $\alpha_1\beta_2$ dimer interface, whereas a complete neutralization of the charge results in a compaction of the overall structure. The βGlu^{7}–βLys^{132} salt bridge appears to play a role in supporting the appropriate charge balance that in turn maintains the A helix-H helix scaffolding and the proper T state hinge.

The UVRR spectrum from the double mutant Hb βE6V/E7A indicates an enhanced separation in the A helix-E helix tertiary contact, as reflected in a weakening of the hydrogen bond between βTrp^{15} and βSer^{72}. This finding supports the idea that a change in the A helix packing is responsible for the observed decrease in Hb βE6V/E7A polymerization (1, 2). It is not clear whether the weakening of the hydrogen bond between βTrp^{15} and βSer^{72} is purely the result of the local perturbation on the A helix or the combined result of the A helix mutations with the unshielded charge at βLys^{132}. The double mutant, Hb βE6V/E7A, also shows a substantially decreased Y8a band intensity, attributed to an increased separation between the H helix and the F helix. The combined effect is suggestive of a global expansion or loosening of the tertiary structure.

The spectroscopic changes occurring upon addition of IHP to the CO-saturated derivatives of all the species examined is consistent with IHP inducing a general tightening of the overall globin structure. This tightening is reflected in spectroscopic signatures of a strengthened hydrogen bonding between the A and E helices and the H and F helices. At pH 7.35, addition of IHP to the CO saturated derivatives does not perturb the switch region of the $\alpha_1\beta_2$ dimer interface but does induce T state character into the hinge region of all but the βK132A mutants. Thus, the βE7A mutation eliminates the deligation-induced R → T state hinge transition but not the IHP-induced effect on the hinge, whereas the βK132A mutation eliminates the IHP effect but maintains (or even enhances) the deligation-induced change. It follows that attaining the T state conformation at the hinge region of the $\alpha_1\beta_2$ dimer interface can be achieved through different pathways and that these pathways are subject to subtle mutagenic manipulation at sites well removed from the interface.

REFERENCES

1. Lesecq, S., Baudin, V., Kister, J., Marden, M., Poyart, C., and Pagnier, J. (1996) *J. Biol. Chem.* **271,** 17211–17214
2. Lesecq, S., Baudin, V., Kister, J., Poyart, C., and Pagnier, J. (1997) *J. Biol. Chem.* **272,** 15242–15246
3. Asher, S. (1981) *Methods Enzymol.* **76,** 371–413
4. Rousseau, D. L., and Friedman, J. M. (1988) in *Biological Applications of Raman Spectroscopy* (Spiro, T. G., ed) Vol. III, pp. 133–215, John Wiley & Sons, New York
5. Kitagawa, T. (1988) in *Biological Application of Raman Spectroscopy* (Spiro, T. G., ed) Vol. III, pp. 97–131, Wiley & Sons, New York
6. Jayaraman, V., Rodgers, K. R., Mukerji, I., and Spiro, T. G. (1995) *Science* **269,** 1843–1848
7. Wang, D., and Spiro, T. G. (1998) *Biochemistry* **37,** 9940–9951
8. Kitagawa, T. (1992) *Prog. Biophys. Mol. Biol.* **58,** 1–18
9. Rodgers, K., Su, S., Subramaniam, S., and Spiro, T. (1992) *J. Am. Chem. Soc.* **114,** 3697–3709
10. Jayaraman, V., Rodgers, K. R., Mukerji, I., and Spiro, T. G. (1993) *Biochemistry* **32,** 4547–4551
11. Mukerji, I., and Spiro, T. G. (1994) *Biochemistry* **33,** 13132–13139
12. Rodgers, K. R., and Spiro, T. G. (1994) *Science* **265,** 1697–1699
13. Hu, X., and Spiro, T. G. (1997) *Biochemistry* **36,** 15701–15712
14. Sokolov, L., and Mukerji, I. (1998) *J. Phys. Chem. B* **102,** 8314–8319
15. Juszczak, L., and Friedman, J. (1999) *J. Biol. Chem.* **274,** 30357–30360
16. Nagamoto, S., Nagai, M., Tsuneshige, A., Yonetani, T., and Kitagawa, T. (1999) *Biochemistry* **38,** 9659–9666
17. Nagai, M., Wajcman, H., Lahary, A., Nakatsukasa, T., Nagatomo, S., and Kitagawa, T. (1999) *Biochemistry* **38,** 1243–1251
18. Hirsch, R., Juszczak, L., Fataliev, N., Friedman, J., and Nagel, R. (1999) *J. Biol. Chem.* **274,** 13777–13782
19. Hirsch, R. E., Lin, M. J., Vidugirus, G. V., Huang, S., Friedman, J. M., and Nagel, R. L. (1996) *J. Biol. Chem.* **271,** 372–375
20. Juszczak, L., Hirsch, R., Nagel, R., and Friedman, J. (1998) *J. Raman Spectrosc.* **29,** 963–968
21. Bihoreau, M., Baudin, V., Marden, M., Lacaze, N., Bohn, B., Kister, J., Schaad, O., Dumoulin, A., Edelstein, S., Poyart, C., and Pagnier, J. (1992) *Protein Sci.* **1,** 145–150
22. Nagai, K., and Thogersen, H. (1984) *Nature* **309,** 810–812
23. Nagai, K., Perutz, M., and Poyart, C. (1985) *Proc. Natl. Acad. Sci. U. S. A.* **82,** 7252–7255
24. Wang, Y., and Van Wart, H. (1993) *Methods Enzymol.* **226,** 319–373
25. Wang, D., Zhao, X., Shen, T.-J., Ho, C., and Spiro, T. (1999) *J. Am. Chem. Soc.* **121,** 11197–11203
26. Jayaraman, V., and Spiro, T. G. (1995) *Biochemistry* **34,** 4511–4515
27. Nagai, M., Kaminaka, S., Ohba, Y., Nagai, Y., Mizutani, Y., and Kitagawa, T. (1995) *J. Biol. Chem.* **270,** 1636–1642
28. Huang, S., Peterson, E. S., Ho, C., and Friedman, J. M. (1997) *Biochemistry* **36,** 6197–6206
29. Su, C., Park, Y. D., Liu, G., and Spiro, T. G. (1989) *J. Am. Chem. Soc.* **111,** 3457–3459
30. Huang, J., Juszczak, L. J., Peterson, E. S., Shannon, C. F., Yang, M., Huang, S., Vidugiris, G. V. A., and Friedman, J. M. (1999) *Biochemistry* **38,** 4514–4525
31. Chang, C., Simplaceanu, V., and Ho, C. (2002) *Biochemistry* **41,** 5644–5655
32. Kwiatkowski, L. D., Hui, H. L., Wierzba, A., Noble, R. W., Walder, R. Y., Peterson, E., Sligar, S., and Sanders, K. (1997) *Biochemistry* **37,** 4325–4335
33. Peterson, E. S., and Friedman, J. M. (1998) *Biochemistry* **37,** 4346–4357
34. Ishimori, K., Imai, K., Miyazaki, G., Kitagawa, T., Wada, Y., Morimoto, H., and Morishima, I. (1992) *Biochemistry* **31,** 3256–3264
35. Togi, A., Ishimori, K., Unno, M., Konno, T., Morishima, I., Miyazaki, G., and Imai, K. (1993) *Biochemistry* **32,** 10165–10169